VI International Conference on Adaptive Modeling and Simulation
ADMOS 2013
J. P. Moitinho de Almeida, P. D iez, C. Tiago and N. Pars (Eds)

# IMPROVEMENT IN PERFORMANCE PARAMETERS BY SHAPE OPTIMIZATION OF A CONICAL FLOW AROUND DIFFUSER

**M. LENARCIC*, S. ERNE* AND C. BAUER***

*Institute for Energy Systems and Thermodynamics (IET)
Vienna University of Technology
Getreidemarkt 9/E302, 1060 Vienna, Austria
e-mail: markus.lenarcic@tuwien.ac.at, www.iet.tuwien.ac.at

**Keywords:** Optimization, Conical Flow Around Diffuser, 3D Flow, Performance Parameter, Turbulence Model

**Abstract.** *This work aims to develop a fully automated shape design optimization of a 3D conical flow around diffuser with fixed main dimensions surrounded by a turbulent incompressible flow. The optimization process is based on OpenFOAM-1.6-ext in combination with a meta-model assisted evolutionary algorithm (MAEA). To improve the global diffuser performance, typical cost functions are considered describing the corresponding operation of the diffuser. The inner and outer contours of the 3D conical flow around diffuser walls are each independently parameterized with a smooth Bézier-Spline of $4^{th}$-order. To provide an additional degree of freedom for the optimization, the inner and outer diffuser wall are either splitted into two continuous segments. Enabling a discontinuous transition in flow direction, the resulting effect on the flow behavior and performance parameters as well are investigated. The obtained results are additionally compared with simulation results of a commercial code.*

## 1 INTRODUCTION

Diffusers are mounted downstream of turbine impellers to convert the remaining kinetic energy into pressure by decelerating the flow. The flow rate of the medium passing through the turbine is significantly affected by the diffusers geometry. In consequence, measures like geometrical restrictions must be taken to avoid adverse flow.
For this reason, a fully automated shape design optimization of a 3D conical diffuser with fixed main dimensions surrounded by turbulent incompressible free flow has been developed for improving performance parameters such as pressure recovery coefficient and diffuser efficiency. By using a fully 3D mesh, any three dimensional effects like intermittently appearing flow separation can be captured. A metamodel assisted evolutionary algorithm (MAEA) is embedded in the standalone optimization tool EASY [1], which interacts with the mesh motion- and CFD-solver included in the CFD-package OpenFOAM-1.6-ext. Regarding the optimization, reasonable cost functions characterizing the proper operation of the diffuser are considered, such as total pressure loss $\Delta p_{tot}$ and pressure recovery coefficient $C_p$. For mesh motion, diffuser wall shapes are parametrized with a smooth Bézier-Spline of $4^{th}$-order, see Fig. 2 (top). For providing the possibility of establishing a so-called shock-diffuser at the diffuser outlet during optimization, an additional degree of freedom is implemented according to Fig. 2 (bottom) in order to investigate the influence of a discontinuity transition at the inner and outer diffuser wall. To preserve appropriate inlet profiles, a fully 3D physical model of the hydrokinetic turbine with implemented original diffuser are steady-stately calculated and 1D-profiles for velocity- and turbulence-quantities of the swirling flow exiting the impeller are assumed as inlet boundary condition. Strong convex curvature occurring in the diffuser necessitates the application of a modified two equation $k-\omega$ shear stress model with streamline-curvature correction (SST-CC $k$-$\omega$) [6] to capture the highly turbulent flow.
In order to evaluate the optimization process, the pressure recovery coefficient obtained by optimized geometry is compared with results from both original- and conical diffuser geometries and with commercial code. For comparison purposes and for getting better insight into the diffuser performance under realistic flow conditions, a free surface flow simulation is done. Additionally, some basic aspects of swirling flow through conical diffuser enhancing vortex formations are briefly mentioned.

### 1.1 Numerical Details and Boundary Conditions

The flow simulations consider an incompressible isothermal fluid flow using the Reynolds-averaged Navier-Stokes (RANS) method. For the steady-state pressure-velocity coupling the SIMPLE-Algorithm was used, for the transient one the PISO-Algorithm. For all convective terms a $2^{nd}$-order interpolation scheme as well as a $1^{st}$-order implicit Euler scheme for time discretization was applied. To enhance stability of the SIMPLE velocity-pressure coupling, moderate under-relaxation factors were defined. The mesh was generated in accordance to the $y^+$-criterion ($y^+ \geq 30$) required from turbulence models using a standard wall function. During mesh movement, a constant cell height of cells near the moving walls was ensured.

## 2 METHODS AND NUMERICAL SETUP

The set of boundary conditions was defined as usual for ducted single phase flow. To avoid numerical oscillations at the domain outlet a fixed mean static pressure boundary condition was prescribed. For the turbulence quantities and static pressure zero gradient boundary conditions were chosen at the domain inlet. A 1D-profile including $U_1(r)$, $k_1(r)$ and $\omega_1(r)$ was given at

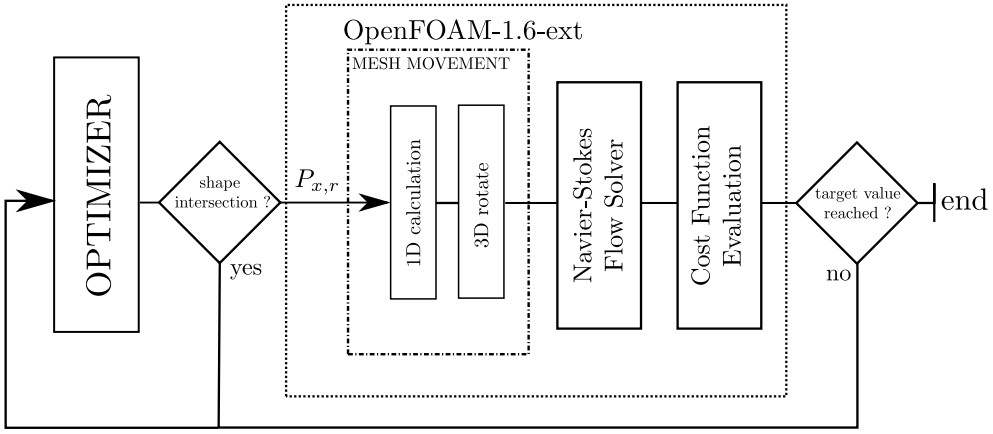


Figure 1: Work flow of the optimization process.

the diffuser inlet, assuming an axisymmetric inflow. At the ambient inlet, a permanent bulk velocity $U_{1AMB}$ (free flow velocity) was predefined, see Fig. 2. To prescribe the turbulent quantities at the ambient inlet, the turbulent kinetic energy $k$ and the dissipation rate $\omega$ were set with $k = 1.5(U_{1\text{AMB}}I)^2$ and $\omega = C_\mu^{0.75}k^{1.5}/l_t$. Based on previous studies, the turbulent intensity $I = 0.03$ and an uniform turbulent mixing length $l_t = 0.01m$ were expected at the domain inlet. The distance between the solid diffuser wall and the free slip boundary defined at the farfield was chosen sufficiently big, see Fig. 4 . For demonstrating the effect of the diffuser geometry contour, a comparison between optimized- ($\text{OPT}_\text{D}$/$\text{OPT}_\text{C}$ with or without either one discontinuous transition along the inner and outer diffuser walls), original- (ORIG) and conical (CON) wall shapes with same grid refinement was simulated.

### 2.1 Mesh Movement and Parameterization

For the parameterized boundary mesh movement, a mesh motion solver based on Laplacian smoothing was applied. A variable quadratic diffusivity was prescribed during deformation to keep distortions in the boundary region as low as possible. The vertices of the inner and outer wall shapes of the 3D conical flow around diffuser were each independently parameterized with a smooth Bézier-Spline of $4^{th}$-order and rotated by $360°$ yielding a 3D circular contour. Such a curve of degree $N$ is defined by the following parameterization

$$\mathbf{X}(t) = \sum_{i=0}^{N} \binom{N}{i} (1-t)^{N-i} t^i \mathbf{P}_i, \text{ with } t \in [0,1] \tag{1}$$

and is therefore ideally suited for varying the order of the Bézier-Spline. To ensure clarity about the effect of a discontinuous transition along the inner and outer diffuser walls, their contours were parametrized both with a polynomial of $3^{rd}$-order and $1^{st}$-order, enabling a discontinuity, as can be seen in Fig. 2 (bottom). On the other hand, the contour is defined by a Bézier-Spline of $4^{th}$-order causing smooth contour shapes, see Fig. 2 (top). Due to restrictions on the optimizer's directives, the inlet- and outlet coordinates of the diffuser wall shapes were assumed to be constant, that means $P_0$, $P_N = const$. Additionally, with considering a discontinuity along the diffuser walls, $P_{N-1}$ was also assumed to be constant ($P_{N-1} = const$), see Fig. 2 (bottom). All integrated values describing the diffuser characteristic were calculated at the diffuser inlet $R_1$ and -outlet $R_2$.

As a compromise between accuracy and computational costs the diffuser walls are only parameterized with a smooth Bézier-Spline of max. $4^{th}$-order , which have already provided

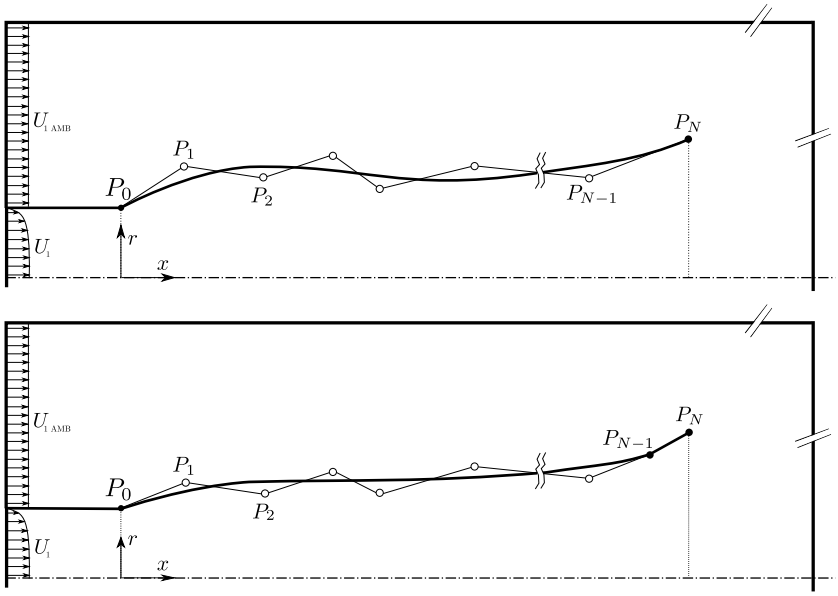


Figure 2: Interior diffuser boundary with a Bézier-Spline Parametrization of $N$-order (top) or with an additional Bézier-Spline Parametrization of $1^{st}$-order for considering a discontinuity (bottom); (dashed) evaluation plane.

appropriate results for a quasi 2D wedge type diffuser [9].

### 2.2 Mesh Independence Study

For the given problem a mesh independence study with the conical diffuser was performed to determine the required number of computational cells. Calculations of $\Delta p_{\text{tot}}$ at three stages of grid refinement ($h = 1, 2, 4$) were introduced and opposed to an estimated value $f_{h=0}$ from a Richardson Extrapolation [8] with higher order based on the lower order values $f_{h_i}$, see Tab. 1 and Fig. 3. The estimation $f_{h=0}$ becomes

$$f_{h=0} \approx f_{h=1} + \frac{f_{h=1} - f_{h=2}}{r^p - 1} \tag{2}$$

whereas $r$ is the grid refinement and $p$ the formal order of accuracy of the algorithm. The order of convergence is defined as $p = ln(f_{h=4} - f_{h=2})/(f_{h=2} - f_{h=1}))/ln(2)$ and $h$ prescribes the grid spacing. So, one can estimate the value of a quantity $f$ as the grid spacing goes to zero ($h \to 0$). The Grid Convergence Index (CGI), based upon a Richardson error estimator, represents a

| $Grid$ | $h_i$ | $r = h_{i+1}/h_i$ | $f_{h_i}/f_{h=4}$ |
|---|---|---|---|
| - | - | - | $m^2/s^2$ |
| $A^{fine}$ | 1 | 2 | 0.4546 |
| $B$ | 2 | 2 | 0.4747 |
| $C$ | 4 | – | 1 |

Table 1: Three different grid refinement stages with the integration variable $\Delta p_{\text{tot}}$ as quantity of $f_{h_i}$, Normalized Grid Spacing $h_i$.

| $\lvert\epsilon_{21}\rvert$ | $\lvert\epsilon_{42}\rvert$ | $\epsilon_{21}/\epsilon_{42}$ | $p$ | $GCI_{21}$ | $GCI_{42}$ |
|---|---|---|---|---|---|
| $10^{-1}$ | $10^{-1}$ | – | – | % | % |
| 0.42 | 5.25 | 0.08 | 4.70 | 0.22 | 2.62 |

Table 2: Grid Convergence Index for three integration variables at different mesh refinements.

measurement of the difference between the computed data and the asymptotic numerical value.

The CGI on the fine grid reads

$$CGI_{fine} = \frac{F_s|\epsilon_{21}|}{r^p - 1}, \tag{3}$$

while the CGI of a coarser one is defined as $CGI_{coarse} = F_s|\epsilon_{42}|r^p/(r^p-1)$, wherein the relative error is $\epsilon_{i+1,i} = (f_{h_{i+1}} - f_{h_i})/f_{h_i}$. The incorporated safety factor of $F_s = 1.25$ is suggested in several works. As can be seen from Tab. 2, the convergence ratio $R = \epsilon_{21}/\epsilon_{42} < 1$ shows a monotonic convergence behavior.

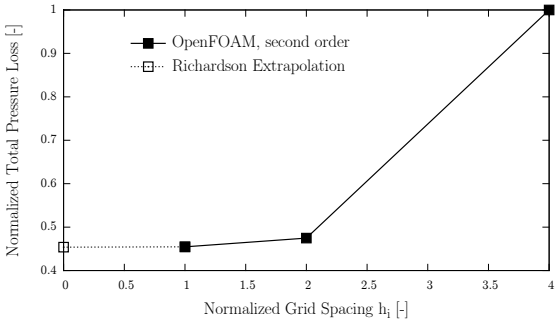


Figure 3: Calculated $\Delta p_{\text{tot}}$ at different refinement stages against the asymptotic approximation obtained from the Richardson Extrapolation.

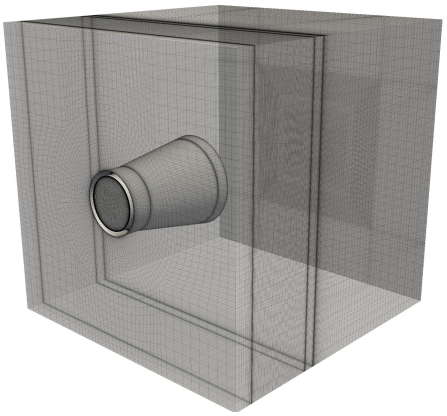

Figure 4: Computational area of the conical diffuser.

Due to high computational costs during the time-consuming optimization process, the medium size grid ($h = 2$) with about $2 \times 10^6$ nodes was chosen for all calculations. Figure 4 illustrates a typical computational grid used in the present work.

### 2.3 Flow Characteristics

In order to predict the diffuser efficiency, the well known pressure recovery coefficient $C_p$ as an averaged integrated value was used during optimization. Based on theoretical considerations, a simple estimation of $C_p$ can be derived from geometrical conditions only. After applying the Bernoulli-Equation along a streamline from in- to outlet of the diffuser, the resulting ideal pressure recovery coefficient is given by

$$C_{pi} = 1 - \frac{1}{AR^2}, \tag{4}$$

which only depends of the area ratio $AR = D_2^2/D_1^2$ of the diffuser geometry.

The diffuser performance is characterized by the flow averaged pressure recovery coefficient using the normalized total kinetic energy $0.5|U_1|^2$ at the diffuser inlet

$$C_p = \frac{\int_{\psi_2} p_2 \, d\psi_2 - \int_{\psi_1} p_1 \, d\psi_1}{0.5 \int_{\psi_1} |U_1|^2 \, d\psi_1} \tag{5}$$

where $\psi$ is the face flux at the calculation sections. Based on flowrate weighted values, the inlet swirl is defined by the swirl number

$$S = \frac{\int_{\psi_1} U_{ax} U_\theta r d\psi_1}{R_1 \int_{\psi_1} U_{ax}^2 d\psi_1}, \tag{6}$$

whereas the characteristic radius is the diffuser inlet radius $R_1$. The quantity represents the ratio between angular and stream-wise momentum of the diffuser flow at the domain inlet. To ensure simulation accuracy, all cost functions and performance quantities used in the optimization process are averaged.

Due to swirl inflow, centrifugal forces gain a radial pressure distribution in the diffuser, which leads to a low pressure level at the diffuser centerline. At a certain level of inlet swirl, defined by the swirl number $S$, the arising of an axisymmetric streamwise vortex may be a cause of worsening the diffuser performance. With increasing swirl, the pressure level at the diffuser centerline decreases due to low velocity. So, the resulting dead water region reduces the effective diffuser cross section similar to an annular discharge channel. To quantify the influence of this cross-sectional area reduction the variable $D_{2,vc}$ is introduced characterizing the magnitude of the vortex core:

$$AR_{vc} = \frac{D_2^2 - D_{2,vc}^2}{D_1^2} \tag{7}$$

Hence the corrected ideal pressure recovery coefficient is given now by $C_{pi,vc} = 1 - 1/AR_{vc}^2$. Here, the outer diameter $D_{2,vc}$ was taken from a simple post simulation process, which extracts the vortex core region inside the diffuser. Information about the bounding streamline between main flow and vortex flow was obtained by applying a simple filter function of $|u| \to 0$, which was found to be sufficiently accurate for the present study. Interpolation between those calculated discrete points was done by a modest polynomial interpolation $D_{2,vc}(x) = \sum a_i x^i$ $(i = 0 \dots 3)$.

Since the diffuser geometry strongly influences the occurrence of undesired flow phenomena inside the diffuser, the basic geometry specifications of the present diffuser are characterized by parameters like the non-dimensional length $L/D_1$ and the non-dimensional area ratio $AR$ for conical diffusers, as defined in Eq. 8 and 9.

$$\frac{L}{D_1} \approx 1.7 \tag{8}$$

$$AR = \left(1 + 2\frac{L}{D_1} tan\theta\right)^2 \approx 2.9 \tag{9}$$

### 2.4 Optimization Strategy

Optimization of hydraulic flow devices often involves time and is associated with computational cost, especially when optimizing complex 3D geometries. One efficient possibility is applying an evolutionary algorithm (EA) with an inexact pre evaluation procedure for optimization. By introducing low-cost surrogate evaluation models, also called ”metamodels”,

a significantly decreasing number of calls can be reached. Thus, this method aims to reduce computational resources caused by the evaluation code, here CFD. Further details on the subject can be found in [2]. The optimization software EASY used in this study, is based on Metamodel-Assisted-Evolutionary-Algorithms, widely denominated as MAEA, which are presented thoroughly in [3]. Another time-saving technique for global optimization is called the hierarchical distributed MAEA (DMAEA) yielding a drastic reduced number of evaluations by introducing separately handled subpopulation.

To find the optimal hydraulic layout of a 3D conical diffuser a $(\mu, \lambda)$ MAEA is coupled with the open source CFD software package OpenFOAM-1.6-ext solving in parallel. This technique subdivides the main population (offspring, parent and elite) into three different sub populations, which are interacting among themselves over specific evolution operators. As discussed above, metamodels are highly beneficial towards performance issues and need a database to store the individuals. The implemented MAEA utilizes locally trained metamodels, for which neighbor entries in the database are selected. $\lambda$ radial basis function networks [4] are applied to pre evaluate the population members before they are evaluated by problem specific tools and stored in the database.

## 3 TURBULENCE MODEL VALIDATION

Outflow of an axial turbine is often characterized by a strong circumferential flow component, which can alter the flow regime in the diffuser radically. Appearing angular momentum leads to streamline curvature as well as a radial pressure gradient, which results in a low pressure field at the diffuser centerline. Turbulent axisymmetric flow with swirl appears in several industrial flow devices and needs to be addressed in a more specific way.

Thus, a turbulence model with modified production terms of the turbulent kinetic energy following [6] was implemented into OpenFOAM-1.6-ext, which considers the turbulence aniso tropy of swirling flow. The correction factor $f_{\text{corr}}$ was defined in Eq. 10 and multiplied in the transport equations for both $k$ and $\omega$. In simple terms, it should be noted that $r^*$ and $\widetilde{r}$ represent a function of the fluid normal stress $\mathbf{S}$ and shear stress tensor $\mathbf{\Omega}$. Flow with vanishing streamline curvature therefore yields $f_{\text{corr}} = 1$.

$$f_{\text{corr}} = (1 + c_{r1})\frac{2r^*}{1 + r^*}\left(1 - c_{r3}\tan^{-1}(c_{r2}\widetilde{r}\right) - c_{r1} \tag{10}$$

The turbulence models were briefly tested using a three-dimensional case [5] at a moderate swirl level of $S = 0.388$ (see Eq. 6). As can be seen in Fig. 11, the original SST $k$-$\omega$ model underestimates the angular velocity $W$ in the wall near region, whereas the center line velocity is predicted well. The corrected model shows a slight improvement of the angular velocity although an overestimation at the end of the divergent part is observed, leading to a minor backflow in the center region.

## 4 RESULTS

### 4.1 IDEAL PRESSURE RECOVERY COEFFICIENT $C_{pi}$

To point out the influence of strong dead water flow at the diffuser center line on the effective cross-sectional area, the optimized geometry is taken as an representative example. The curves of different ideal pressure recovery coefficients $C_{pi}(x)$ at swirl inflow ($S = 0.07$, calculated with Eq. 6), are shown in Fig. 6. The development of $C_{pi}$ using the common formulation Eq. 4 shows the best pressure recovery and ends up at a value over $0.9$. Based on the consideration of

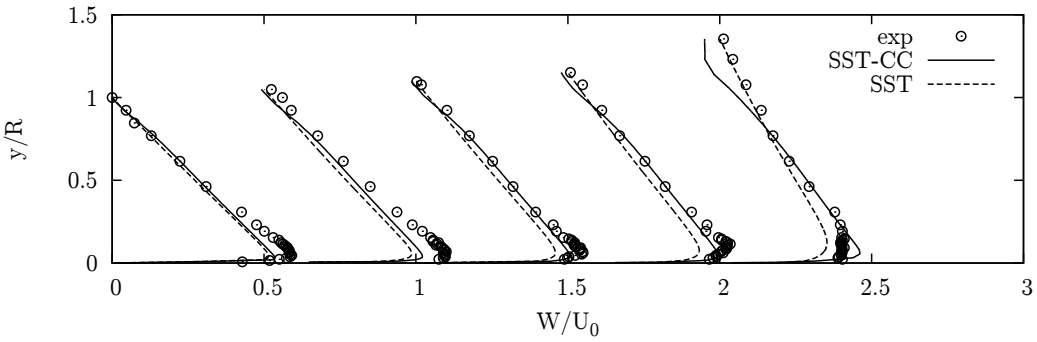


Figure 5: Comparison of circumferential velocity $W$ using standard SST $k$-$\omega$ and SST-CC $k$-$\omega$.

a corrected area ratio $AR_{vc}$ (Eq. 7), the obtained $C_{pi,vc}$ clearly shows a weakening trend towards diffuser performance of about $6.2\%$, readily seen in Fig. 6. Figure 7 illustrates the shape of the optimized wall shape and vortex boundary streamline respectively. Both curves bear a certain geometrical resemblance to one another.

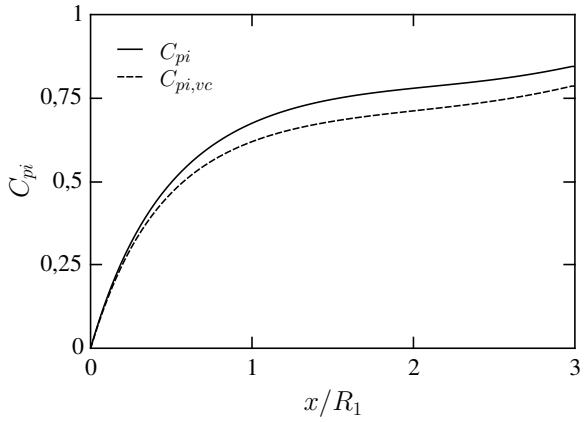


Figure 6: Development of the pressure recovery coefficient in the conical diffuser.

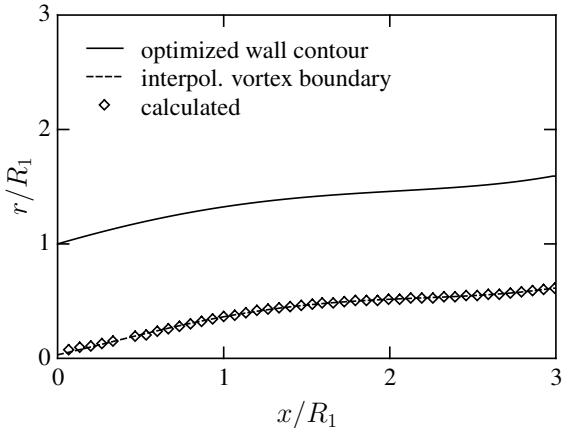


Figure 7: Wall contour of the diffuser wall and the interpolated vortex core bounding streamline.

## 4.2 OPTIMIZATION

Table 3 shows steady-stately and transiently calculated pressure recovery coefficients $C_p$ for the different diffuser geometries ORIG, CON, $\text{OPT}_\text{C}$ and $\text{OPT}_\text{D}$. Due to steady-state optimization process using $C_p$ as cost-function, a significant increase of $C_p$ compared to the original- and conical diffuser is gained, yielding a concave-flat-convex curved wall shape, as can be seen in Fig. 8. Comparable results have been already obtained in [9, 10], for additional qualitatively descriptions of the results see [10, 11, 13].

In order to take time depending factors into account, transient investigations with a maximum Courant Number of $Co_{max} = 1$ were performed using a monitoring period of 15 seconds from reaching a converged state. Comparing steady-state- and transient results, significant differences in $C_p$ occur with the optimized geometries $\text{OPT}_\text{C}$ and $\text{OPT}_\text{D}$. While $\text{OPT}_\text{C}$ achieves a higher $C_p$ during steady-state optimization process, the value drops more than for $\text{OPT}_D$ if transient effects are regarded. This can be attributed to a higher sensitivity of the steady $\text{OPT}_\text{C}$-contour with respect to time-dependent influences. Compared to the original diffuser ORIG, the improvements of $C_p$ according to transient simulations correspond to a respective percentage

| $Geo$ | $C_{pS}$ | $C_{pT}$ | $\Delta C_{pT}$* | $\Delta C_{pS-T}$** |
|---|---|---|---|---|
| - | - | - | % | % |
| $ORIG$ | 0.459 | 0.438 | 0.00 | 4.60 |
| $CON$ | 0.534 | 0.506 | 15.5 | 5.20 |
| $OPT_C$ | 0.680 | 0.580 | 32.4 | 14.7 |
| $OPT_D$ | 0.643 | 0.592 | 35.2 | 7.90 |

Table 3: Comparison of the steady-stately calculated pressure recovery coefficient $C_{pS}$ and the transiently calculated one $C_{pT}$ for the different geometries ORIG, CON, $\text{OPT}_\text{C}$ and $\text{OPT}_\text{D}$; difference of $C_{pT}$ related on ORIG geometry (*), difference between steady-state and transient results (**).

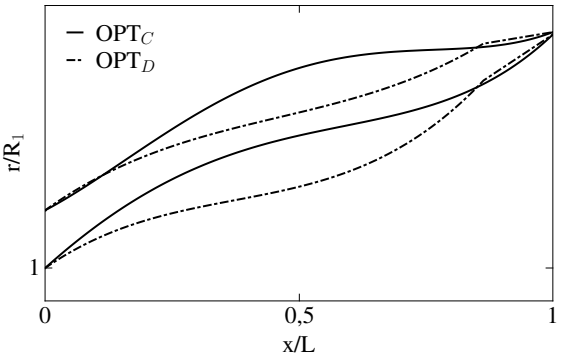


Figure 8: Optimized diffuser wall shapes $\text{OPT}_\text{C}$ and $\text{OPT}_\text{D}$ using $C_p$ as cost-function.

of approximately $32\%$ for $\text{OPT}_\text{C}$ and $35\%$ for $\text{OPT}_\text{D}$ - and related to the conical diffuser CON of approximately $15\%$ for $\text{OPT}_\text{C}$ and $17\%$ for $\text{OPT}_\text{D}$. Figure 9 and Fig. 10 show the influence of different diffuser wall shapes on the established flow pattern. A strongly pronounced hub vortex formation displaces the remaining fluid towards the diffuser walls leading to an energy enrichment of the boundary layer, which in turn prevents flow separation in those regions.

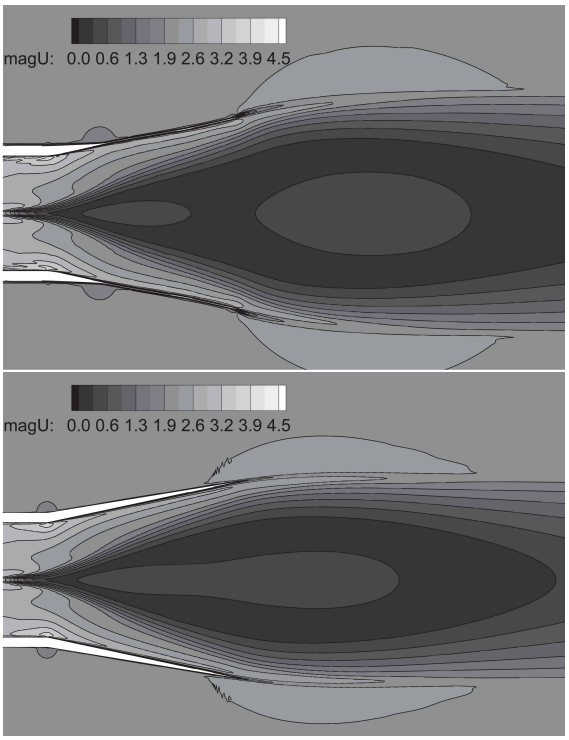


Figure 9: Comparison of the transiently calculated velocity U for the diffuser geometries ORIG and CON.

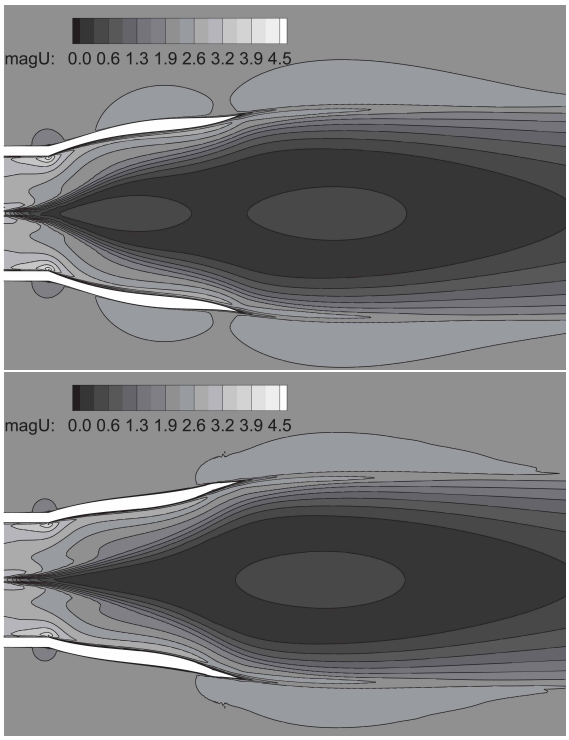


Figure 10: Comparison of the transiently calculated velocity U for the optimized diffuser geometries $\text{OPT}_\text{C}$ and $\text{OPT}_\text{D}$.

Since hub vortex structures are less developed for $\text{OPT}_\text{D}$, a higher diffuser efficiency is reached than for the other optimized geometry $\text{OPT}_\text{C}$. Additionally, the discontinuity at the

$OPT_D$-contour stabilizes the flow and time sequence of $C_p$ and $\Delta p_{tot}$ are about half the size of amplitudes for $OPT_C$. Despite transient effects, an almost steady flow field is induced with a standard deviation for $C_p$ and $\Delta p_{tot}$ of $SD_{C_p} < 3 \times 10^{-3}$ and $SD_{\Delta p_{tot}} < 5 \times 10^{-3}$ for all investigated geometries.

Compared to transient results from commercial code, differences of $C_p$ and $\Delta p_{tot}$ are less than 1.5%.

### 4.3 FREE SURFACE FLOW

Hydrokinetic turbines driven by river current often have mounted a diffuser or augmented channel unit downstream improving the flow characteristics of the turbine. To study the diffuser characteristics under more realistic conditions, free surface flow simulations in a gravitational field with appropriate inflow conditions were performed. A constant inflow water level and a unique flow velocity for both fluid and air was prescribed at the ambient inlet boundary. The side walls were defined again as symmetric planes.

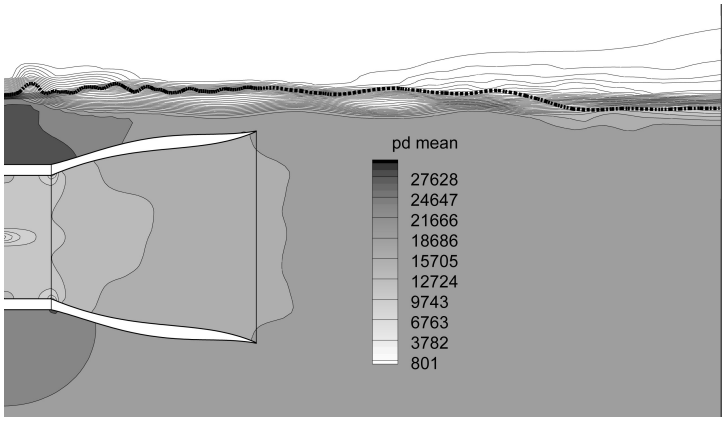


Figure 11: Contour plot of static pressure distribution $p_d$ at y-z plane for the optimized geometry $OPT_C$. (dashed line) instantaneous contour of free surface; $p_d$ in $N/m^2$.

The diffuser inflow conditions remain the same as those used in the single phase flow. Numerical details and discretization methods the used flow solver is based on, can be found in [7]. For the present study a coarsened block-structured mesh was used, however, with the same boundary layer resolution. The maximum Courant Number was $Co_{max} < 0.25$ during the transient simulation of 60 seconds, after reaching a quasi steady-state flow solution. Compared with single phase studies using the same computational settings, the free surface flow simulation tends to stronger fluctuations in the diffuser characteristics. As the simulation additionally takes account of the hydrostatic pressure distribution and free surface stress forces, the variation over time of $C_p$ is increased significantly.

Figure 11 illustrates the static pressure distribution including the low pressure region in the outer air flow. Even in the two phase simulation an improvement of $C_p$ due to wall shape optimization comes apparent. Compared to the conical diffuser CON, the $OPT_C$ shows an improvement corresponding to a respective percentage increase of approximately 10%. A comparison between the time-averaged pressure recovery coefficient of the single phase- and two phase simulation shows that they are broadly in the same range, as can be seen in in Tab. 4.

Figure 12 draws streamlines of both CON and $OPT_C$ diffuser, where the simulation using the optimized wall shape shows less single vortices in the backflow region. Also, the streamwise growth of the vortex core inside the optimized diffuser is significantly weaker than in the

| $Geometry$ | $C_{p_{1Ph}}$ | $C_{p_{2Ph}}$ | $\Delta C_{p_{1Ph-2Ph}}{}^{*}$ |
|---|---|---|---|
| - | - | - | % |
| $CON$ | 0.506 | 0.492 | 2.8 |
| $OPT_C$ | 0.580 | 0.548 | 5.5 |

Table 4: Comparison of transiently calculated pressure recovery coefficient $C_p$ for the geometries CON and $\text{OPT}_\text{C}$; single phase- (1Ph) and two phase simulation (2Ph); difference of $C_p$ related on results from 1Ph calculation (*).

original diffuser observing a more stable vortex structure. Both plots present a reduction of the diffuser area due to vortex formations at the centerline and a strongly disturbed flow after the diffuser.

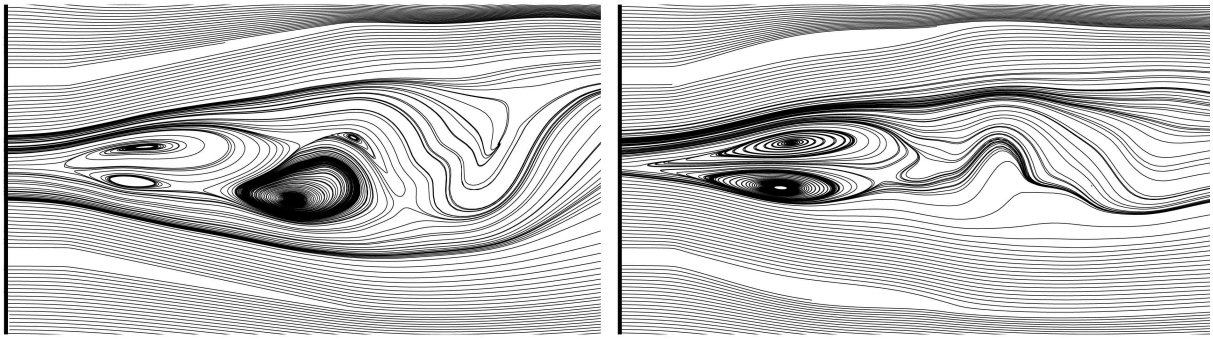

Figure 12: Time averaged velocity streamlines projected on y-z plane; left: conical contour (CON), right: optimized contour ($\text{OPT}_\text{C}$).

## 5 CONCLUSION

In this work an efficient coupling of OpenFOAM-1.6-ext with the optimization tool EASY using a generalized metamodel assisted evolutionary algorithm (MAEA) is outlined. During fully automated shape design optimization of a 3D conical flow around diffuser, the inner and outer diffuser walls are each independently parameterized with a smooth Bézier-Spline of max. $4^{th}$-order. A modified version of the SST $k$-$\omega$ model is applied to capture streamline curvature effects inside the diffuser flow. The influence of a discontinuity transition at the inner and outer diffuser wall is carried out as well. The resulting optimized geometries show a comparable diffuser efficiency, leading to a moderate increase of $C_p$ compared to the original- and conical geometry. Compared to the original diffuser ORIG, the improvements of $C_p$ according to transient simulations correspond to a respective percentage of approximately $32\%$ for $\text{OPT}_\text{C}$ and $35\%$ for $\text{OPT}_\text{D}$ - and related to the conical diffuser CON of approximately $15\%$ for $\text{OPT}_\text{C}$ and $17\%$ for $\text{OPT}_\text{D}$. The qualitative progress of the optimized curve shapes are quite similar to those of previous diffuser investigations by [12, 9, 10]. Transient single phase simulations cause an almost steady flow field with negligible standard deviations of $C_p$.
A comparison between the time-averaged pressure recovery coefficient $C_p$ calculated by transient single phase- and two phase simulations for conical and optimized diffuser geometries shows appropriate agreements with each other. However, the free surface flow simulation has shown significantly stronger pressure fluctuations appearing more realistic, but is found to be too time consuming for an evaluation code application.

Further studies are aimed at developing a wall shape optimization of an oval 3D flow around

diffuser using Bézier-Surfaces for parameterization. Additionally, a simplified wall blowing concept is applied on the turbine hub in order to reduce vortex formations.

## REFERENCES


[1] K.C. Giannakoglou: The EASY (Evolutionary Algorithms SYstem) software, http://velos0.ltt.mech.ntua.gr/EASY(2008).

[2] K.C. Giannakoglou: Design of optimal aerodynamic shapes using stochastic optimization methods and computational intelligence. *Progress in Aerospace Sciences*, 38(11) (2002), 43–76.

[3] I.C. Kampolis and K.C. Giannakoglou: Distributed Evolutionary Algorithms with Hierarchical Evaluation. *Engineering Optimization*, 44(11) (2009), 1037–1049.

[4] S. Haykin: Neural Networks: A Comprehensive Foundation. *Pearson Education*, - (2001).

[5] P. D. Clausen, S.G. Koh, and D.H. Wood *Measurements of a swirling turbulent boundary layer developing in a conical diffuser*. Fluid Mechanics and Heat Transfer, 6 (1993), 39-48.

[6] P. E. Smirnov and F. R. Menter *Sensitization of the SST Turbulence Model to Rotation and Curvature by Applying the Spalart-Shur Correction Term*. Journal of Turbomachinery, 131 (2009), 041010-1 - 041010-8.

[7] H. Rusche: Computational fluid dynamics of dispersed two-phase flows at high phase fractions. PHD Thesis, *Imperial College of Science, Technology and Medicine, UK* 2002.

[8] L.F. Richardson: The deferred approach to the limit. Part I. Single lattice. Part II. Interpenetrating lattices. Philosophical Transactions of the Royal Society of London. Series A, Containing Papers of a Mathematical or Physical Character, 226 (1927), 299361

[9] S. Erne, M. Lenarcic, C. Bauer and S.A. Kyriacou: Shape optimization of a flow around circular diffuser in a turbulent incompressible flow, ECCOMAS, 2012

[10] M. Lenarcic, S. Erne and C. Bauer: Efficiency improvement by performing shape optimization of a circular flow around diffuser in a turbulent incompressible flow, $17^{th}$ International Conference on Hydropower Plants, 2012

[11] Y. Ohya and T. Karasudani: A Shrouded Wind Turbine Generating High Output Power with Wind-lens Technology, Energies, 2010, ISBN 0-933283-00-8

[12] B. Schmandt and H. Herwig: Diffuser and Nozzle Design Optimization by Entropy Generation Minimization. *Entropy*, 13 (2011), 1380–1402.

[13] D. Japikse: TURBOMACHINERY DIFFUSER DESIGN TECHNOLOGY, Concepts ETI Inc., Norwich, 1984,